*Environ. Water Eng., 2025, 11(3), 326-335* DOI: 10.22034/ewe.2024.477555.1964

EWE

**Environment and Water Engineering**

**Homepage: www.jewe.ir**

ISSN: 2476-3683

# Numerical analysis of geometrical and mechanical characteristics of the sliding mass influences on impulsive wave generation in dam reservoirs

Fateme Maleki[1]✉, Jalal Bazargan[1], and Ahmad Darudi[2]

[1]Department of Civil Engineering, Faculty of Engineering, University of Zanjan, Zanjan, Iran
[2]Department of Physics, Faculty of Science, University of Zanjan, Zanjan, Iran

**ARTICLE INFO**

**Paper Type:** Research Paper

**Received**: 08 September 2024
**Revised:** 22 October 2024
**Accepted**: 04 November 2024
**Published**: 20 December 2024

**Keywords**
Flow-3D Model
Impact Velocity
Mass Volume
Mass Width
Wave Characteristics

***Corresponding author:**
F. Maleki
✉ f.maleki@znu.ac.ir

**ABSTRACT**

Impulsive waves caused by landslides into lakes and dam reservoirs strike the shores and dam bodies as large waves. The most important factor in their generation is the transfer of momentum from the mass to the water, which can cause damage. Therefore, understanding the factors influencing this phenomenon is a constant concern for researchers. In this study, the simultaneous effect of the mechanical and geometrical characteristics of the landslide mass was investigated. The investigations were carried out in two parts. First, a laboratory model was used to generate a wave to verify the performance of the numerical Flow-3D model, and then four variables of material, width, thickness, and impact velocity of the mass in wave generation were investigated numerically. The results showed that by increasing the thickness of the mass by 20%, the wavelength increased by about 25%. The volume of the mass was more effective than the width or thickness variables separately, and a mass with a larger volume generated a larger wave. According to the results, increasing the velocity of the mass led to the production of a larger wave, which was related to the material of the mass. With a 14% increase in impact velocity, a 50% increase in wavelength was created in the rigid mass and a 30% increase in the porous mass, which showed that in the rigid mass, the effect of velocity on the wave magnitude was greater.

**Highlights**

- Mass volume impacts wave size more than width/thickness alone.
- Higher impact velocity increases wavelength by up to 50%.
- Solid masses generate larger waves compared to porous masses.
- Surface tension inclusion improves numerical model accuracy.
- Porosity reduces wave energy by damping momentum transfer.

**Citation:**
Maleki, F., Bazargan, J., & Darudi, A. (2025). Numerical analysis of geomechanical influences on impulsive wave generation in dam reservoirs. *Environment and Water Engineering*, *11*(3), 326-335. doi: 10.22034/ewe.2024.477555.1964

## 1. Introduction

The catastrophic generation of high-impulsive waves resulting from large solid masses sliding into dam reservoirs and lakes poses a significant hazard. These waves, upon propagating through the reservoir and impacting dam structures, can cause substantial damage. Therefore, a precise and scientific understanding of this phenomenon and its influencing parameters is crucial for the protection of infrastructure, human life, and environmental resources both around and downstream of dam sites. This phenomenon has been consistently associated with substantial economic and human losses worldwide. Notable examples include the Vaiont Dam reservoir landslide in Italy, the Lituya Bay event in Canada, and occurrences in New Guinea, all of which resulted in significant economic and human costs (Wang et al., 2019). The Vaiont Dam landslide, with an approximate volume of 270 MCM, created a wave that overtopped the dam, leading to the death of 2,000 people in the downstream valley (Takagi et al., 2019). In 1958, a 30 MCM landslide at Lituya Bay generated a wave that reached a height of 524 m above sea level, destroying nearby facilities. More recently, a 3 MCM rock landslide in 2007 at Kahlice Lake in British Columbia, Canada, produced a wave that destroyed vegetation up to 38 m above the shoreline, resulting in a significant accumulation of wood debris at the lake outlet (Grilli et al., 2019). A recent

review studying the impact of massive landslides into stagnant waters discussed this phenomenon in terms of the location, natural factors affecting it, and the environmental and infrastructural damage they cause (Marin et al., 2024). Landslide-induced waves can be investigated from different aspects. Various researchers have employed analytical (Zhou and Teng, 2010; Ma et al., 2012), numerical (Wu et al., 2024; Yi et al., 2023; Lo, 2023), and laboratory (Huang and Chen, 2020; Bolin et al., 2023; Liu et al., 2023; Rubin et al., 2023) methods to describe influencing factors from geotechnical, geological, and hydraulic perspectives. They have also provided relationships for estimating and predicting the characteristics of these impulsive waves. In the past, computational fluid dynamics has been utilized to investigate landslide- induced waves and various parameters of the sliding mass. Notably, Flow-3D, Open Foam, and Fluent software have been frequently used in previous studies (Heidarzadeh et al., 2020).

Evers et al. (2019) conducted a laboratory study examining the variables affecting wave characteristics in three-dimensional conditions and proposed equations for predicting wave velocity, length, and height. Bregoli et al. (2017) investigated water surface profiles resulting from the impact of porous and rigid masses in a three-dimensional laboratory model. Zhang et al. (2020) numerically examined the influence of reservoir geometry on wave characteristics. Chen et al. (2023) explored this phenomenon on a real scale in a landslide-prone area in China using numerical modeling. Heller et al. (2008) analyzed the effect of scale and forces in this phenomenon, concluding that water depths in laboratory studies should be greater than 20 cm to mitigate scale effects.

Kim et al. (2012) compared the results of commercial models with laboratory observations in a three-dimensional numerical study and found that results of numerical models, except at the location of wave formation, showed acceptable agreement. Li et al. (2021) used numerical modeling to examine the forces associated with subsurface landslides and the impact of wave height and velocity on single objects in water, demonstrating that the effect of height on the interaction force was significant at low velocities. Romano et al. (2023) developed a rheological model to study impulsive waves generated by granular mass slides, modeling the energy and momentum transfer process between the mass and water. Sabeti et al. (2024), in a novel approach, developed assumptions and modeling processes featuring different mechanisms and calibrations that showed high accuracy and efficiency in simulating the sliding of rigid masses and its near-field effects.

A review of existing research reveals that despite the presence of various laboratory and numerical models, the geometry of a landslide mass within a three-dimensional water body, and its consequential impact on wave generation and propagation, remains under-explored. Furthermore, there is a notable lack of published information regarding the influence of landslide mass parameters and numerical modeling that incorporates surface tension effects on impulsive wave phenomena. Consequently, this research aimed to numerically investigate the geometrical parameters of landslide mass width and thickness, along with their combined effect on mass volume. Additionally, mechanical parameters such as porosity and impact velocity of the landslide mass were analyzed using Flow-3D software, while accounting for the effect of surface tension to ensure numerical model accuracy.

## 2. Materials and Methods

This research focused on the generation and propagation of waves, commencing with the introduction of the governing equations related to fluid motion, followed by a discussion of the modeling approach using Flow-3D software. A sensitivity analysis of grid cell sizes was performed to evaluate the accuracy of the computations and the validity of the numerical model, using experimental data for verification. After confirming the accuracy of the numerical model in simulating the phenomena of interest, models with varying geometries of the landslide mass were developed, and the results were compared with findings from existing literature.

### 2.1 Governing equations and numerical method

The modeling of waves generated from landslides was conducted using the three-dimensional Navier-Stokes equations implemented in Flow-3D version 11.02. This comprehensive study examined the characteristics of wave generation and propagation resulting from landslide movements in reservoir environments. The model employed the Volume of Fluid (VOF) method to solve for incompressible flow and incorporated the RNG turbulence model, which is effective for accurately modeling single-phase flow and sediment-laden flow dynamics (Kim et al., 2020). The VOF method facilitated the definition of geometric regions within a structured mesh, allowing parameter values to be represented based on the average magnitude of each volume element. The flow equations, specifically the Navier-Stokes equations, are defined as conservation of mass and momentum (Tu et al., 2023):

$$\nabla u = 0 \tag{1}$$

$$\frac{\partial u}{\partial t} + u.\nabla u = \frac{-\nabla P}{\rho} + \nu.\nabla^2 u + g \tag{2}$$

where $u$ is the velocity field, $P$ is the pressure field, $\rho$ is the density, and $t$ is time. The surface tension included in this simulation through Flow-3D acts as a force at the interface between gas and liquid or between two immiscible liquids.

**Table 1** Experimental parameters

| Parameters, unit | Values |
|---|---|
| Still water level (m) | 0.75 |
| Water basin sizes (length×width) (m) | 12.5×6.5 |
| Mass sizes (length×width) (m) | 1.5×0.5 |
| Mass weight (kg) | 350 |
| Mass density (kg/m$^3$) | 1870 |
| Mass porosity | 0% |
| Mass thickness (m) | 0.35 |

The characteristics of the porous mass were specified in the physics section of the software as “porous media.” In the geometry and meshing section, the sliding mass component was incorporated as a porous entity. The physics of the porous medium within the software supports various applications, allowing for the definition of porosity, permeability, and moisture absorption for each component in the model’s geometry. By default, porosity is set to 1, indicating no

resistance to flow and that the entire volume is available for fluid passage. In this study, to simulate a porous mass, the porosity value was reduced to 0.5.

### 2.2 Laboratory model

The experimental setup included a sliding mass, a wave tank, and optical instruments to measure wave characteristics, located in the hydraulics laboratory at Zanjan University, Iran. The dimensions of the wave tank were 12.5 m in length, 6.5 m in width, and 1 m in height. The mechanical specifications, dimensions, mass, and geometry of the setup are summarized in Table 1.

In this laboratory model, a cubic steel box filled with a fixed volume of pure cement was utilized to generate waves through sliding. This box was designed to slide down a slope with a 60-degree angle under its weight to produce waves. Fig. 1a illustrates the configuration of the wave tank and the sliding mass. A perspective measurement method, a branch of image processing, was employed to record the characteristics of the generated waves. As depicted in Fig.1-c, this method required a digital camera and points on the surface, represented by green dots, to track the wave's movement and determine its speed. These points were created using laser light spots.

In this method, video recordings captured the moment when the wave crest reached the first row of marked points, and the passage of the wave crest from the second row was also recorded. The wave speed was derived by dividing the distance by the time taken for the crest to traverse between the two rows of lasers. Fig.1-d shows the placement and angle of the laser points mentioned earlier. Due to excessive turbulence and interference from colliding waves about 70 cm from the tank's side walls, recording wave speed proved challenging.

Schematic representations of the experimental equipment, the parameters studied related to impulsive waves, and the arrangement of lasers for surface tracking are presented in Fig. 1. The parameters of impulsive waves examined in this study include the sliding distance of the mass to the water surface (D), wave height (H), wave amplitude ($a_m$), initial water height in the tank (h), and the angle of mass sliding (α).

**Fig. 1** Geometry of model a) laboratoatry basin, b) parameters in schematic Lab. side view, c) parameters in schematic Lab, top view, and d) placement of lasers

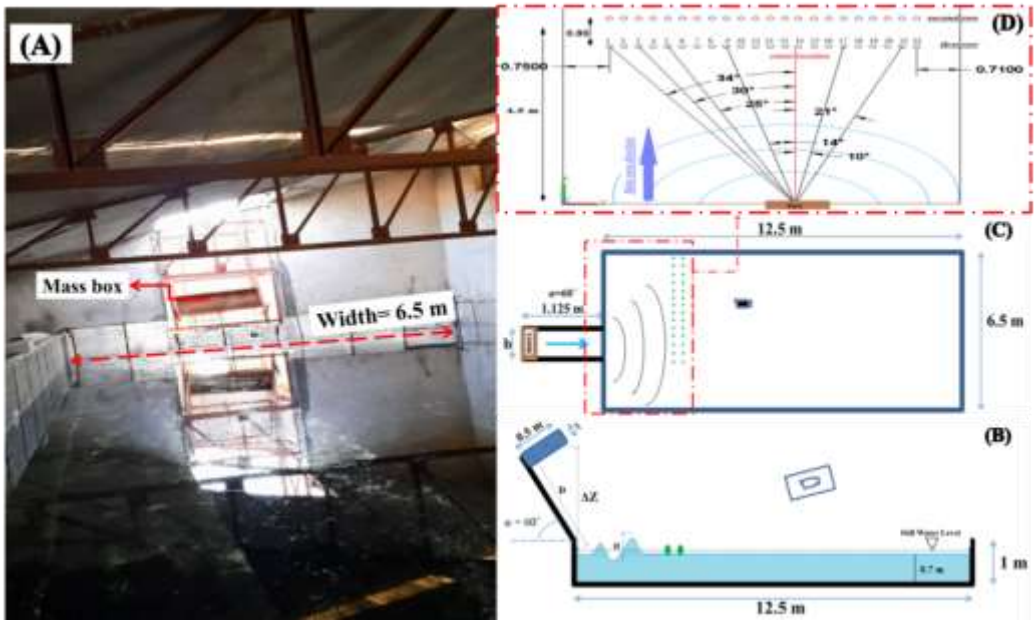


### 2.3 Validation of the numerical model

To validate the numerical model and its underlying hypotheses, data from the experiments outlined in the previous section were utilized. The propagation of impulsive waves generated by landslides in still water was modeled in three dimensions. In the laboratory study, wave speeds were accurately measured at a distance of 4 m from the impact location. These values were used for model validation along the x-axis at points corresponding to the locations of the laser light spots.

For the simulations, it was critical to examine the sensitivity of the results to changes in cell dimensions and the computational grid. In the validation models, the depth of the still water in the tank was set to 75 cm, and the mesh included the air volume above the water surface to visualize the surface waves generated by the mass movement. Three different mesh sizes were tested, as shown in Fig. 2, which compares the water movement speeds in both the numerical and experimental models.

To analyze the sensitivity of the numerical model, cell sizes for the solution field were set to 1, 3, and 5 cm. Modeling was performed for each mesh size, once with surface tension physics enabled and once without. The average absolute error percentages and simulation execution times are summarized in Table 2. The absolute error values in this table reflect the differences in wave speeds resulting from the mass's impact with the water surface, compared to the laboratory measurements.

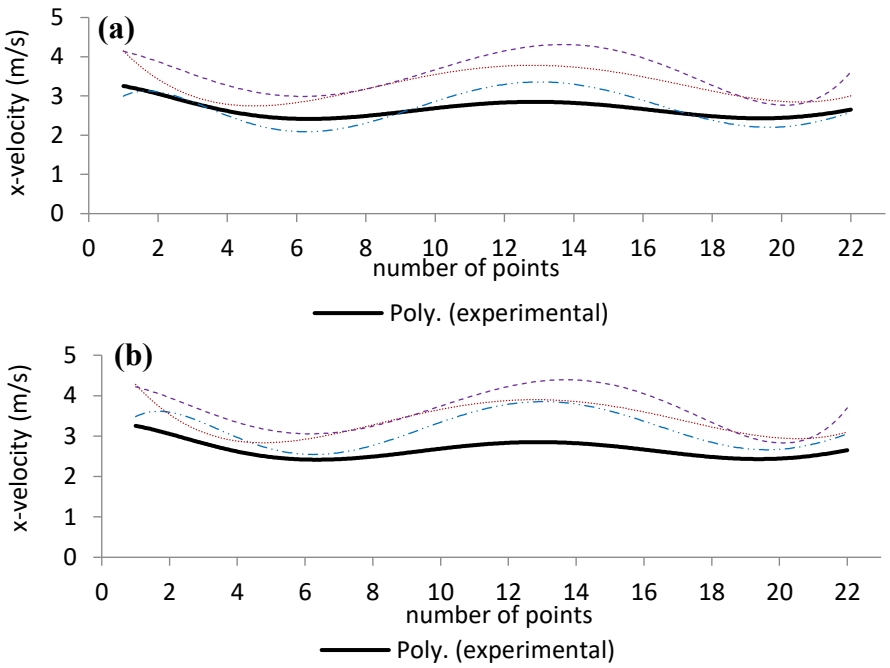


**Fig. 2** Comparisons of measured and simulated wave velocity in various mesh sizes: a) with surface tension and b) without surface tension

**Table 2** Sensitivity analysis of the model

| Model No. | Mesh size (cm) | Number of mesh cells | Physics of surface tension on Flow-3D | Run time (H:M) | Mean Absolute Percentage Error (%) |
|---|---|---|---|---|---|
| 1 | 1 | 81,250,000 | active | 41:50 | 13 |
| 2 | | | Inactive | 39:20 | 19 |
| 3 | 3 | 3,062,448 | active | 25:40 | 22 |
| 4 | | | Inactive | 24 | 27 |
| 5 | 5 | 650,000 | active | 4:50 | 33 |
| 6 | | | Inactive | 4:20 | 35 |

As presented in Table 2, reducing the cell size from 5 to 1 cm decreased the simulation error for the cases both without and with surface tension, from 35% to 17% and from 33% to 13%, respectively. Additionally, simulation times increased significantly, from approximately 290 minutes to 2510 minutes for the case with surface tension and from 260 minutes to 2360 minutes for the case without surface tension. In Computational Fluid Dynamics (CFD) modeling, the Courant condition serves as the convergence criterion that must equal one, indicating that information in the solution field moves cell by cell in one time step. The Courant number is influenced by mesh size, time step, and mesh quality, and ensuring stability in chaotic phenomena often requires minimizing the time step as much as possible. Flow-3D software allows adjustments to ensure convergence in the Courant condition.

Considering surface tension in the numerical modeling significantly enhances calculation accuracy. This research demonstrated that modeling in Flow-3D with surface tension physics enabled yields better accuracy across all mesh sizes. A comparison of modeling accuracy in this study with findings by Maleki and Bazargan (2024) showed that the effect of surface tension is more pronounced in smaller tank dimensions. The average error percentage increased with larger mesh sizes, indicating a mismatch with laboratory samples, as larger sizes reduced the representation of small details in fluid regions. In essence, finer mesh sizes result in greater accuracy in estimating the effects of surface tension.

To evaluate the numerical model's accuracy, the mean percentage of absolute error was calculated. The permissible error for modeling wave phenomena when a numerical model is validated against laboratory data is typically accepted at 20% (NTHMP, 2012). In research conducted by Kim et al. (2020), this value was reported as 35% for the development of the Flow-3D and TSUNAMI3D models.

Increasing the number of mesh cells raises computational complexities and modeling times, necessitating a balance between mesh size and duration. Based on acceptable error values from various researchers for engineering simulations, a mesh size of 1 cm was chosen for optimal economic efficiency. Moreover, considering surface tension in the simulation did not significantly increase simulation time, allowing for more accurate modeling. Adequate precision must be ensured in the aspect ratio of the mesh and the correct solver selection for pressure in the model.

Overall, the results indicated that this numerical model was sufficiently accurate for conducting this research, particularly regarding wave speed, which was well predicted by the model.

The simulation results displayed a strong correlation with laboratory data.

### 2.4 Numerical model

The impulsive wave generated by the landslide mass into the tank was modeled using Flow-3D software. For numerical modeling, the entire flow domain was 12.5 m in length, 6.5 m in width, and 75 cm in depth. The fluid within the tank was defined as water, with a density of 1000 kg/m³ at a temperature of 20°C, and the slope angle of the landslide was fixed at 60 degrees. The dimensions of the sliding mass, characterized as a solid block, varied in this study. Additionally, granular materials shaped like rectangular prisms, with dimensions similar to the solid mass but the same volume, were modeled. Given that the porosity of the sliding mass influenced the generated wave upon impact, a granular material with a porosity of 50% was employed for this assessment.

As detailed in Table 3, a total of 16 models were designed and implemented in Flow-3D, based on variations in the width, thickness, and speed of impact of the sliding mass while considering different mass types and the conditions of surface tension and solid mass.

**Table 3** Characteristics of numerical models

| $V_s$=4.2 m/s | $V_s$=3.7 m/s | t*[m] | Parameters | | |
|---|---|---|---|---|---|
| 9 | 1 | 0.15 | 1 | b* [m] | Solid mass |
| 10 | 2 | 0.25 | | | |
| 11 | 3 | 0.15 | 1.2 | | |
| 12 | 4 | 0.25 | | | |
| 13 | 5 | 0.15 | 1 | b [m] | Porous mass |
| 14 | 6 | 0.25 | | | |
| 15 | 7 | 0.15 | 1.2 | | |
| 16 | 8 | 0.25 | | | |

b: mass length; t: mass thickness, $V_s$:mass impact velocity.

Throughout the study, the traveled distance of the mass in each direction relative to the still water surface was kept constant. The acceleration and speed of the masses were derived from Eqs. 3 and 4, and defined as input parameters in the moving objects model (Xue et al., 2019; Fritz et al., 2004) .

$$a_s = \frac{2D}{t_s^2} \quad (3)$$

$$v_s = \sqrt{2g\Delta z\left(1-\tan\delta\cot\alpha\right)} \quad (4)$$

Where D represents the slip distance, α is the slip angle, t is the slip duration, Δz is the elevation difference from the mass location to the water surface, and δ is the internal friction angle of the mass. An accurate definition of the required variables in the software is crucial for numerical models. Table 4 lists the essential parameters that users must define for modeling in Flow-3D. To ensure stability in the simulations, FLOW-3D applies the Courant condition, which ensures that the model's convergence remains efficient. This value is derived from Eq. 5:

$$C = \frac{U\Delta t}{\Delta x} \quad (5)$$

Where Δt is the time step and Δx is the grid cell size. For boundary conditions, parameter values were set for symmetric and wall conditions according to Eqs. 6 and 7:

$$\frac{\partial u}{\partial x} = 0 \quad \text{and} \quad \frac{\partial p}{\partial x} = 0 \quad (6)$$

$$u = 0 \quad \text{and} \quad \frac{\partial p}{\partial x} = 0 \quad (7)$$

**Table 4** Model values in the simulation process

| Model parameters | | Values |
|---|---|---|
| Finish time (s) | | 10 |
| Turbulence model | | RNG |
| Moving object model | | Collision GMO |
| Mesh size (mm) | | 10 |
| Boundary* condition | $X_{max}$ | S |
| | $X_{min}$ | W |
| | $Y_{max}$ | W |
| | $Y_{min}$ | |
| | $Z_{max}$ | S |
| | $Z_{min}$ | W |
| Contact angle (deg) | | 60 |
| Mass density (kg/m³) | | 1900 |
| Entrainment rate coefficent | | 0.5 |
| Mass impact velocity (m/s) | x | 2.2,1.85 |
| | y | 0 |
| | z | 3.7,3.2 |

* S: symmetry ; W: wall

The wall condition was applied to all regions surrounding the pool and its bottom, while the symmetry condition ensured that flow remained symmetrical along that boundary. The turbulence model used in this research was the RNG model, selected for its accuracy and applicability in free-surface flows (Choi et al., 2007; Sabeti and Heidarzadeh, 2022). To determine the accuracy of the numerical model, Eq. (8) was employed to calculate the mean percentage of the absolute

error between the computed speed and that obtained from the laboratory data.

$$M = \frac{1}{n}\sum_{t=1}^{n}\left|\frac{A_t - F_t}{A_t}\right| \quad (8)$$

where $A$ represents the actual value and $F$ represents the predicted value.

## 3. Results and Discussion

In this study, an initial numerical model was validated against laboratory results, after which various samples were modeled and the results extracted. Waves were generated using two types of sliding masses: a solid block and a granular mass. The characteristics of the initial wave formed upon the mass's impact with the water surface, as well as the mechanisms of its propagation, were analyzed by examining key wave parameters. The four main variables investigated were mass geometry (width and thickness), porosity, and the impact speed of the sliding mass. These factors significantly influence modeling results yet are often overlooked. Table 5 presents the wave height and wavelength values for each model. Notably, the values extracted from the Flow-3D model were taken along the central axis (y = 3.5 m) of the geometry and sliding mass, since the surface profile near the walls was affected by wave amplification and interference due to the impact against the walls and subsequent reflection. An analysis of this phenomenon and its effects on wave propagation constitutes a separate topic. Below, the effects of various parameter changes on the geometric characteristics of the wave were discussed in detail.

**Table 5** wave characteristics (m) of models

| Model NO. | 1 | 2 | 3 | 4 | 5 | 6 | 7 | 8 | 9 | 10 | 11 | 12 | 13 | 14 | 15 | 16 |
|---|---|---|---|---|---|---|---|---|---|---|---|---|---|---|---|---|
| Wave length | 3.31 | 4.15 | 3.78 | 4.59 | 2.5 | 2.87 | 2.65 | 2.91 | 5.07 | 5.59 | 5.31 | 6 | 3.12 | 4.3 | 3.55 | 4.84 |
| Wave height | 0.13 | 0.164 | 0.15 | 0.187 | 0.09 | 0.106 | 0.10 | 0.12 | 0.209 | 0.239 | 0.22 | 0.25 | 0.12 | 0.171 | 0.138 | 0.198 |

### 3.1 Effect of mass geometry

As shown in Fig. 3a, the width and thickness of the impacting mass significantly influenced the generated amplitude and wavelength. As the width of the mass increased, both amplitude and wavelength also increased, as detailed in Table 5. For instance, at an impact speed of 3.7 m/s, an increase in thickness from 0.15 m to 0.25 m (a 66% increase) resulted in wavelength increases of 25% and 22% for mass widths of 1 m and 1.2 m, respectively. Additionally, at thicknesses of 0.15 m and 0.25 m, a 20% increase in width from 1 m to 1.2 m led to wavelength increases of 15% and 11%, respectively. This trend can be attributed to the larger volume of water displaced by the wider mass, which allows the force applied to be distributed over a greater area, resulting in a longer wave front. Clearly, the effect of mass width on wavelength was more pronounced than that of mass thickness, as a threefold increase in width resulted in only a 10% change in wavelength, consistent with the experimental results of Heller and Spinneken (2013).

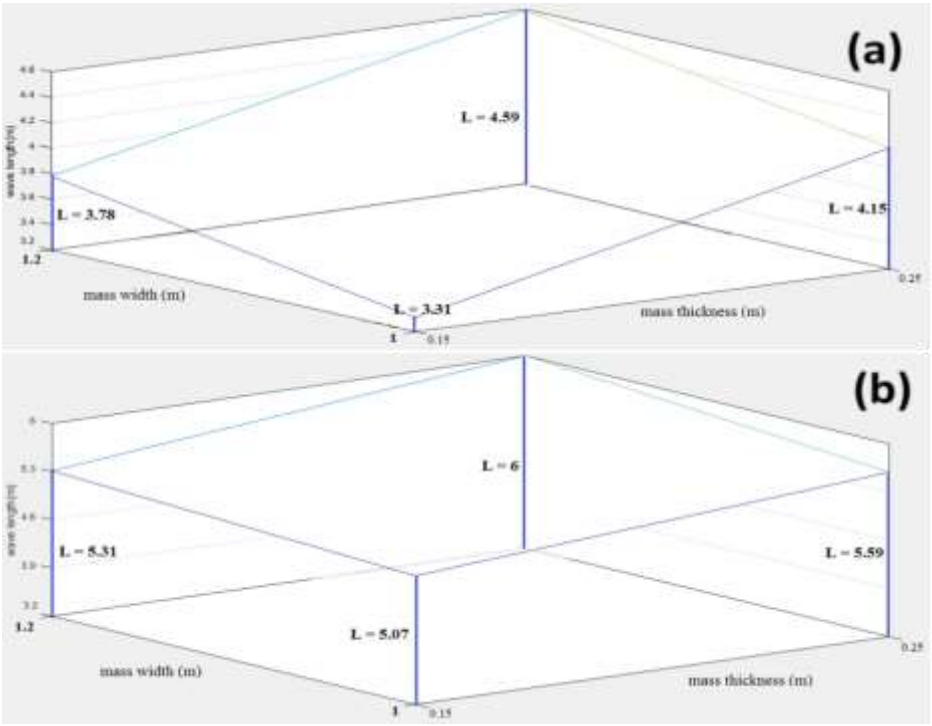


**Fig. 3** Effect of the mass width and thickness on wavelength: a) V=3.7 m/s and b) V=4.2 m/s

This research also considered mass volume as a new geometric parameter. It was determined that, irrespective of the separate effects of width and thickness, a greater mass volume consistently resulted in a larger impact wave. These findings are illustrated in Fig. 4, where the wavelength values for different mass volumes are shown. At the maximum volume change from 0.075 to 0.15 m³, the wavelength increased from 3.31 to 4.59 m. Thus, using the characteristic wave values in Table 5 and the experiments listed in Table 3, variations in wavelength and wave height can be derived relative to changes in the dimensions of other sliding masses.

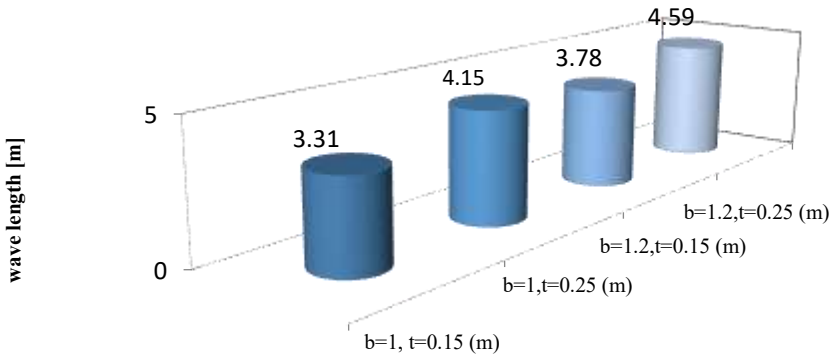


**Fig. 4** Comparison of the mass volume, V=3.7, solid mass

### 3.2 Effect of the impact speed of the mass on the water surface

The impact speed of the sliding mass against the still water surface also affected the characteristics of the produced wave. The initial wave amplitude increased with mass speed, as did the speed of wave propagation, since more energy was transferred to the water. As illustrated in Fig. 5, the wavelength values increased with speed. In this study, a 14% increase in mass impact speed corresponded to average wavelength increases of 2.2 m for solid conditions and 2.1 m for porous conditions across different volumes. Specifically, for the solid mass, increasing the speed from 3.7 m/s to 4.2 m/s resulted in wavelength increases of 40% and 31% for the minimum and maximum mass volumes, respectively. For the porous mass, these increases were noted at 26% and 10%, respectively.

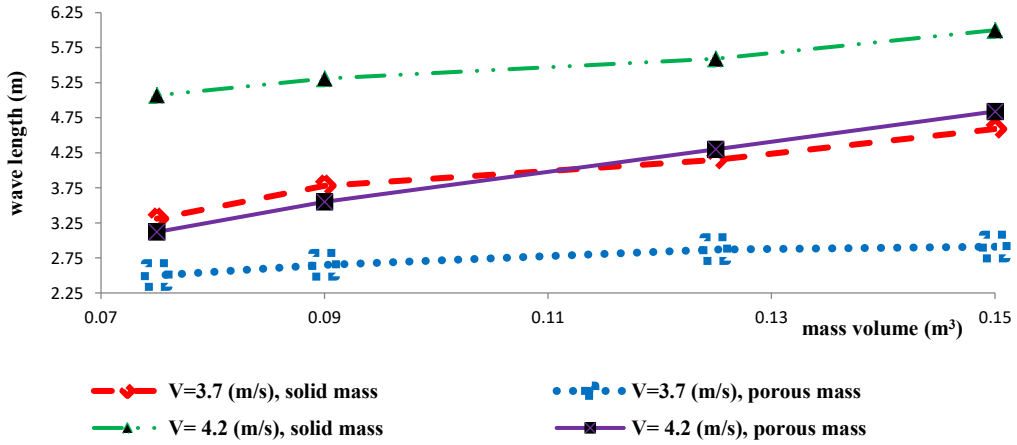


**Fig. 5** Effect of mass impact velocity for various mass volumes

Consequently, the effect of mass speed was more pronounced for solid materials. Solid masses tend to carry and transfer greater momentum, and in the momentum conservation equation, higher velocity changes are associated with greater transferred momentum. For equal volumes, the porous mass has less overall mass due to the presence of air voids, resulting in reduced momentum transfer upon impact.

### 3.3 Effect of material composition of the sliding mass

The effects of the material composition of the sliding mass, specifically varying porosities, were also examined. As shown in Fig. 6, the wavelength values generated by the solid mass were consistently greater than those of the porous mass at equal speeds and volumes. This could be attributed to the porosity of the mass and how the water surface interacts with the voids and grains. The results indicated that increased porosity in the sliding mass resulted in smaller waves with less energy. The voids in the mass absorbed impact energy, thereby reducing momentum transfer to the water surface, similar to the behavior of a damper.

For the solid mass, average wavelength increases of 41% and 45% were observed as the speed increased from 3.7 m/s to 4.2 m/s, highlighting the importance of speed as a factor in wave generation.

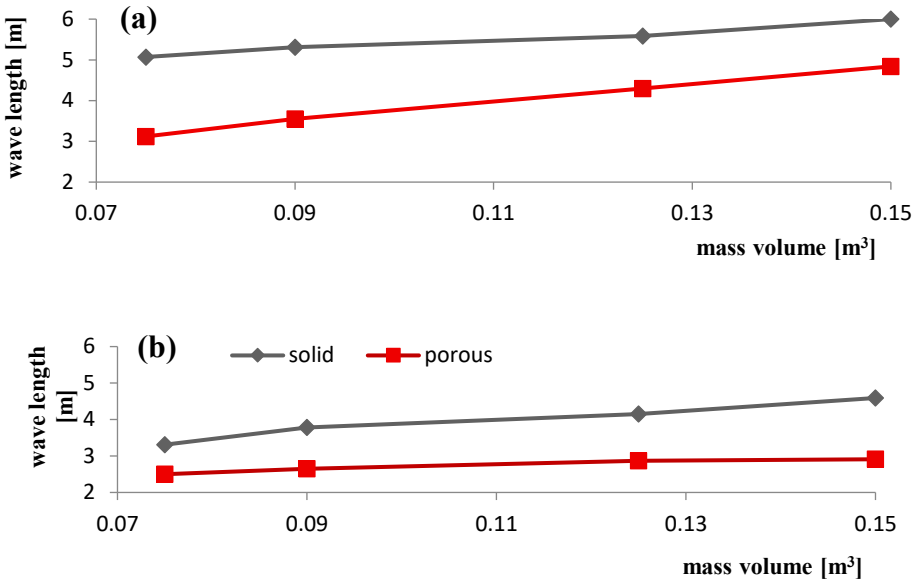


**Fig. 6** mass porosity effect of mass for various mass volumes: a) V= 4.2 m/s and b) V=3.7 m/s

## 4. Conclusion

This study examined the geometric parameters of width and thickness of the mass, as well as the combined variable of mass volume, alongside mechanical parameters including porosity and the impact speed of the sliding mass against the water surface. This analysis was conducted using a three-dimensional model in Flow-3D software, which was validated against laboratory models. The effect of surface tension on the accuracy of the numerical model was also considered. The comparison of the effects of porosity, mass speed, and mass thickness, as mentioned in previous studies, confirmed the results of this research. The main findings of this study are summarized as follows:

1. A mass with greater width and thickness tended to generate waves with higher amplitudes and longer wavelengths. These waves contained more energy and propagated over longer distances.

2. While mass thickness and width influenced wave characteristics, the effect of mass volume on these geometric parameters was more significant and pronounced. Furthermore, the impact of volume was greater for solid materials than for porous materials.

3. An increase in the impact speed of the mass against the water surface resulted in the generation of larger waves. This augmentation in wave size was related to the material of the mass; for masses with lower porosity percentages, the impact speed had a more substantial effect on wave characteristics. Specifically, the increase in speed led to average wavelength expansions of approximately 35% for solid masses and 17% for porous masses.

4. As the porosity of the sliding mass increased, wave height and speed decreased, while wavelength increased. For solid masses, the average increase in wavelength compared to porous masses was about 42%. This can be attributed to the reduction of momentum transferred from the mass to the water surface during impact, particularly when porosity was low.

Based on the results obtained, it is recommended that the variables of porosity and the volume of potentially sliding masses in dam reservoirs and lakes prone to the risks of this destructive phenomenon be examined further to more accurately predict and derive the characteristics of impulsive waves generated from sliding. Additionally, in a combined model, the interaction effects of porosity and mass speed—both of which are influential factors on momentum—should be investigated.

### Statements and Declarations

### Data availability

Data will be made available on request via email (f.maleki@znu.ac.ir).

### Conflicts of interest

The author of this paper declared no conflict of interest regarding the authorship or publication of this paper.

### Author contribution

F. Maleki: Study design, numerical modeling, and construction and equipment of the laboratory sample, analysis and interpretation of results, writing the text; J. Bazargan: Study design, analysis and interpretation of results, approval of the final text. A. Dorudi: Analysis and extraction of wave characteristics by optical method.

### AI Use Declaration

This study did not incorporate artificial intelligence techniques; instead, all analyses and optimizations were conducted using conventional and widely accepted analytical methods.

**References**


Bolin, H., Yueping, Y., Renjiang, L., Peng, Z., Zhen, Q., Yang, L. & Kaikai, X. (2023). Three-dimensional experimental investigation on hazard reduction of landslide-generated impulse waves in the Baihetan Reservoir, China. *Landslid*es, *20*(9), 2017-2028. DOI: 10.1007/s10346-023-02068-w

Bregoli, F., Bateman, A., & Medina, V. (2017). Tsunamis generated by fast granular landslides: 3D experiments and empirical predictors. *Journal of Hydraulic Research, 55(6)*, 743-758. DOI: 10.1080/00221686.2017.1289259

Chen, X., Jing, H., Li, P., & Fan, Y. (2023, June). Numerical investigation of landslide-generated impulse waves in Yangqu reservoir, China. *In ISOPE International Ocean and Polar Engineering Conference (pp. ISOPE-I). ISOPE*.

Choi, B. H., Kim, D. C., Pelinovsky, E., & Woo, S. B. (2007). Three dimensional simulation of tsunami run-up around conical island. *Coastal Engineering, 54*(8), 618-629. DOI: 10.1016/j.coastaleng.2007.02.001

Evers, F. M., Hager, W. H., & Boes, R. M. (2019). Spatial impulse wave generation and propagation. *Journal of Waterway, Port, Coastal and Ocean Engineering, 145*(3), 04019011. DOI: 10.1061/(ASCE)WW.1943-5460.0000514

Flow Science, Inc. (2023). *Flow-3D user manual* (Version 11.0.2).

Fritz, H. M., Hager, W. H., & Minor, H. E. (2004). Near field characteristics of landslide generated impulse waves. *Journal of Waterway, Port, Coastal and Ocean Engineering, 130*(6), 287-302. DOI: 10.1061/(ASCE)0733-950X(2004)130:6(287)

Grilli, S. T., Tappin, D. R., Carey, S., Watt, S. F., Ward, S. N., Grilli, A. R., ... & Muin, M. (2019). Modelling of the tsunami from the December 22, 2018 lateral collapse of Anak Krakatau volcano in the Sunda Straits, Indonesia. *Scientific Reports, 9(1)*, 11946. DOI: 10.1038/s41598-019-48327-6

Heidarzadeh, M., Ishibe, T., Sandanbata, O., Muhari, A., & Wijanarto, A. B. (2020). Numerical modeling of the subaerial landslide source of the 22 December 2018 Anak Krakatoa volcanic tsunami, Indonesia. *Ocean Engineering, 195*, 106733. DOI: 10.1016/j.oceaneng.2019.106733

Heller, V., Hager, W. H., & Minor, H. E. (2008). Scale effects in subaerial landslide generated impulse waves. *Experiments in Fluid, 44*, 691-703. DOI: 10.1007/s00348-007-0427-7

Heller, V., & Spinneken, J. (2013). Improved landslide-tsunami prediction: effects of block model parameters and slide model. *Journal of Geophysical Research: Oceans, 118*(3), 1489-1507. DOI: 10.1002/jgrc.20099

Huang, J., & Chen, G. (2020). Experimental study on wave impulse and characteristic pressure of a vertical wall with overhanging horizontal cantilever slab. *Ocean Engineering, 217*, 108055. DOI: 10.1016/j.oceaneng.2020.108055

Kim, G. (2012). Numerical simulation of three-dimensional tsunami generation by subaerial landslides (*Doctoral dissertation*). DOI: https://hdl.handle.net/1969.1/148349

Kim, G. B., Cheng, W., Sunny, R. C., Horrillo, J. J., McFall, B. C., Mohammed, F., Fritz, H. M., Beget, J. & Kowalik, Z. (2020). Three dimensional landslide generated tsunamis: Numerical and physical model comparisons. *Landslides, 17*, 1145-1161. DOI: 10.1007/s10346-019-01308-2

Li, R. Y., Chen, J. J., & Liao, C. C. (2021). Numerical study on interaction between submarine landslides and a monopile using CFD techniques. *Journal of Marine Science and Engineering, 9(7),* 736. DOI: 10.3390/jmse9070736

Liu, J., Wang, Y., Xiao, T., Yin, K., Huo, Z., Wang, X., & Tang, Y. (2023). Experimental investigation on nearfield edge wave runups generated by landslides in narrow reservoirs. *Geological Journal, 58*(6), 2268-2282. DOI: 10.1002/gj.4674

Ma, G., Shi, F., & Kirby, J. T. (2012). Shock-capturing non-hydrostatic model for fully dispersive surface wave processes. *Ocean Modelling, 43*, 22-35. DOI: 10.1016/j.ocemod.2011.12.002

Maleki, F., & Bazargan, J. (2024). 3D Numerical Modeling of Impulsive Wave Generation and Propagation by landslides in Dam Reservoir. *Journal of Hydraulic, 20(2),* DOI: 10.30482/jhyd.2024.450808.1698. [In Persian].

Romano, A., Lara, J. L., Barajas, G., & Losada, Í. J. (2023). Numerical modeling of tsunamis generated by granular landslides in OpenFOAM®: A Coulomb viscoplastic rheology. *Coastal Engineering, 186*, 104391. DOI: 10.9753/icce.v37.papers.21

Rubin, W., Wang, Y., Wan, J., Xu, W., Yang, Y., & Wang, H. (2023). Propagation mechanism of deep-water impulse waves generated by landslides in V-shaped river channels of mountain valleys: physical model of regular rigid block. Geofluids, DOI: 10.1155/2023/1743305

Sabeti, R., & Heidarzadeh, M. (2022). A new empirical equation for predicting the maximum initial amplitude of submarine landslide-generated waves. *Landslids., 19*(2), 491-503. DOI: 10.1007/s10346-021-01747-w

Sabeti, R., Heidarzadeh, M., Romano, A., Barajas Ojeda, G., & Lara, J. L. (2024). Three-Dimensional Simulations of Subaerial Landslide-Generated Waves: Comparing OpenFOAM and FLOW-3D HYDRO Models. *Pure and Applied Geophysics, 1-19*. DOI: 10.1007/s00024-024-03443-x

Takagi, H., Pratama, M. B., Kurobe, S., Esteban, M., Aránguiz, R., & Ke, B. (2019). Analysis of generation and arrival time of landslide tsunami to Palu City due to the 2018 Sulawesi earthquake. *Landslides, 16*, 983-991. DOI: 10.1007/s10346-019-01166-y

Tu, J., Yeoh, G. H., Liu, C., & Tao, Y. (2023). Computational fluid dynamics: a practical approach. Elsevier.

Wang, J., Ward, S. N., & Xiao, L. (2019). Tsunami Squares modeling of landslide generated impulsive waves and its application to the 1792 Unzen-Mayuyama mega-slide in Japan. *Engineering Geology, 256*, 121-137. DOI: 10.1016/j.enggeo.2019.04.020

Wu, H., Shi, A., Ni, W., Zhao, L., Cheng, Z., & Zhong, Q. (2024). Numerical simulation on potential landslide–induced wave hazards by a novel hybrid method. *Engineering Geology,* 107429. DOI: 10.1016/j.enggeo.2024.107429

Xue, H., Ma, Q., Diao, M., & Jiang, L. (2019). Propagation characteristics of subaerial landslide-generated impulse waves. *Environmental Fluid Mechanics, 19*, 203-230. DOI: 10.1007/s10652-018-9617-5

Yi, X., Feng, W., Li, B., Yin, B., Dong, X., Xin, C., & Wu, M. (2023). Deformation characteristics, mechanisms, and potential impulse wave assessment of the Wulipo landslide in the Baihetan reservoir region, China. *Landslides, 20*(3), 615-628. DOI: 10.1007/s10346-022-02010-6

Zhang, Y., Li, D., Chen, L., Yin, K., Xiao, L., Fu, X., ... & Leo, C. (2020). Numerical analysis of landslide-generated impulse waves affected by the reservoir geometry. *Engineering Geology, 266*, 105390. DOI: 10.1016/j.enggeo.2019.105390

Zhou, H., & Teng, M. H. (2010). Extended fourth-order depth-integrated model for water waves and currents generated by submarine landslides. *Journal of Engineering Mechanics, 136*(4), 506-516. DOI: 10.1061/(ASCE)EM.1943-7889.0000087